Asiala, Steven and Shand, Neil C. and Faulds, Karen and Graham, Duncan (2017) Surface-enhanced spatially-offset raman spectroscopy (SESORS) in tissue analogs. ACS Applied Materials and Interfaces. ISSN 1944-8244 , http://dx.doi.org/10.1021/acsami.7b09197

This version is available at https://strathprints.strath.ac.uk/61200/

Strathprints is designed to allow users to access the research output of the University of Strathclyde. Unless otherwise explicitly stated on the manuscript, Copyright © and Moral Rights for the papers on this site are retained by the individual authors and/or other copyright owners. Please check the manuscript for details of any other licences that may have been applied. You may not engage in further distribution of the material for any profitmaking activities or any commercial gain. You may freely distribute both the url (https://strathprints.strath.ac.uk/) and the content of this paper for research or private study, educational, or not-for-profit purposes without prior permission or charge.

Any correspondence concerning this service should be sent to the Strathprints administrator: strathprints@strath.ac.uk

The Strathprints institutional repository (https://strathprints.strath.ac.uk) is a digital archive of University of Strathclyde research outputs. It has been developed to disseminate open access research outputs, expose data about those outputs, and enable the management and persistent access to Strathclyde's intellectual output.

This is an open access article published under a Creative Commons Attribution (CC-BY) License, which permits unrestricted use, distribution and reproduction in any medium, provided the author and source are cited.

ACS AuthorChoice

ACS APPLIED MATERIALS & INTERFACES

Research Article

www.acsami.org

Surface-Enhanced, Spatially Offset Raman Spectroscopy (SESORS) in Tissue Analogues

Steven M. Asiala,[†] Neil C. Shand,[‡] Karen Faulds,[†] and Duncan Graham*[,†]

[†]Department of Pure and Applied Chemistry, Technology and Innovation Centre, University of Strathclyde, 99 George Street, Glasgow G1 1RD, United Kingdom

[‡]Defence Science and Technology Laboratory, Porton Down, Salisbury SP4 0JQ, United Kingdom

ABSTRACT: Surface-enhanced, spatially offset Raman spectroscopy (SESORS) combines the remarkable enhancements in sensitivity afforded by surface-enhanced Raman spectroscopy (SERS) with the non-invasive, subsurface sampling capabilities of spatially offset Raman spectroscopy. Taken together, these techniques show great promise for *in vivo* Raman measurements. Herein, we present a step forward for this technique, demonstrating SESORS through tissue analogues of six known and varied thicknesses, with a large number of distinct spatial offsets, in a backscattering optical geometry. This is accomplished by spin-coating SERS-active nanoparticles (NPs) on glass slides and monitoring the relative spectral contribution from the NPs and tissue sections, respectively, as a function of both the tissue thickness and the spatial offset of the collection probe. The results show that SESORS outperforms SERS alone for this purpose, the NP signal can be attained at tissue thicknesses of >6.75 mm, and greater tissue thicknesses require greater spatial offsets to maximize the NP signal, all with an optical geometry optimized for utility. This demonstration represents a step forward toward the implementation of SESORS for non-invasive, *in vivo* analysis.

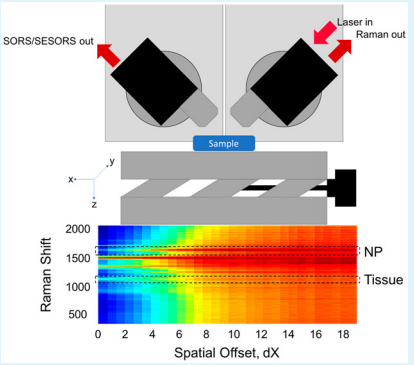

KEYWORDS: *nanoparticles, nanotags, Raman, SORS, tissue analysis*

INTRODUCTION

Surface-enhanced Raman spectroscopy (SERS) is a powerful analytical technique that relies on an enhanced electromagnetic field near the surface of a metal nanostructure to amplify a traditionally weak Raman signal to impressive levels,[1] facilitating detection at the single-molecule limit.[2,3] Theoretical electromagnetic enhancement factors on the order of 10^{10}[,11] have been reported,[4] vastly improving detection limits for a number of SERS-based assays. In addition, the amenable surface chemistry of gold and silver nanoparticles (NPs) has led to the development of biofunctional nanoprobes, optimized for detection both *in vitro* and *in vivo*, with a NP core, Raman reporter, stabilizing layer, and biomolecule functionalization to target specific biomarkers of interest.[5−7]

One drawback of Raman measurements made *in vivo* is the surface selectivity of the measurements; the observed spectrum is dominated by contributions from the surface layer of the sample. While longer excitation wavelengths can be used to enhance tissue penetration and advancements have been made in terms of instruments purpose built for *in vivo* Raman imaging,[8−11] gathering spectral information from the subsurface remains a challenge.[12] One method that allows for collection of spectral information from the subsurface in a multilayered sample is spatially offset Raman spectroscopy (SORS).[13,14] SORS makes use of an applied spatial offset between the points of excitation and collection in a Raman measurement to collect photons that have been scattered by the subsurface medium. Comparisons between the spectra collected with no offset (surface measurements) and those collected with a lateral offset (subsurface measurements) allow one to delineate the differences in composition at depth. SORS of bone tissue has been demonstrated *in vivo* in both mice[15] and humans[16] in an attempt to elucidate composition, with bone signals detected from depths of ≤2 mm.[16]

The field of surface-enhanced, spatially offset Raman spectroscopy (SESORS) has emerged in an attempt to couple the sensitivity afforded by SERS with the subsurface probing of SORS to allow detection at even greater depths, with an eye toward performing measurements *in vivo*. The first successful demonstration of SESORS[17] and subsequent work[18,19] have shown detection of NPs at impressive depths (≤50 mm); however, this work utilized what can be classified as an extreme spatial offset, with a 180° angle between excitation and detection. While these are exciting developments, this is not entirely practical for all applications where researchers might wish to detect SERS NPs at depth through tissue samples where a 180° offset might not be possible. In similar work, Dey et al.[20,21] have demonstrated SESORS with a backscattering geometry for particles injected into a section of proteinaceous tissue at two depths (3−4 and 7−8 mm) and drop-cast under a thin section (1−2 mm) of lipid-rich tissue. Van Duyne et al. have used an optical fiber in a backscattering optical

Received: June 26, 2017
Accepted: June 29, 2017
Published: June 29, 2017

© XXXX American Chemical Society

DOI: 10.1021/acsami.7b09197
ACS Appl. Mater. Interfaces XXXX, XXX, XXX−XXX

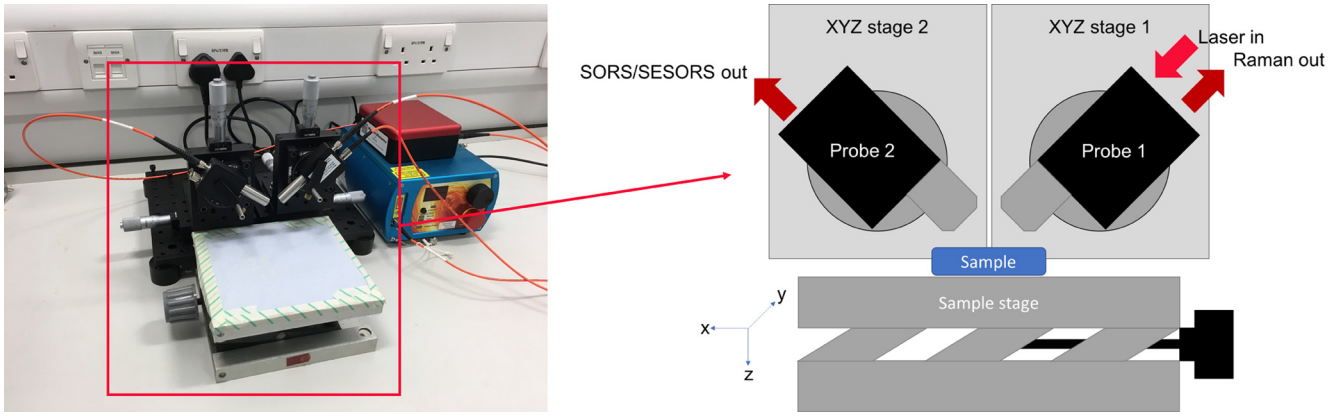

Figure 1. Photograph and schematic of the Raman spectrometer used in SORS and SESORS experiments.

configuration to perform SESORS with rat models, with the use of a film-over-nanosphere substrate serving as the SERS enhancement mechanism.[22,23] Utilizing similar instrumentation, Sharma has demonstrated detection of nanotags through bone of varied thickness, with the signal obtained from NP tags injected into tissue adjacent to the bone.[24] Each of these backscattering studies relies on a single, fixed spatial offset, corresponding to the distance between a central excitation point and an annular arrangement of collection fibers, and/or studies a very limited number of tissue thicknesses. Both spatial offset and tissue thickness need to be studied together in a robust, coherent fashion to clearly demonstrate their relation in SESORS measurements.

Herein, we demonstrate backscattering SESORS through tissue analogues of six known and varied thicknesses, with NP tags as the enhancing medium, measuring spectra at a large number of spatial offsets per tissue thickness. By spin-coating nanotags and characterizing the result, we determined the fixed distribution of the particles in these experiments, allowing a limit of tissue thickness to be established for the optical system as described. In addition, studying multiple tissue thicknesses and many spatial offsets together allows for an explicit understanding of the interrelated effects of the two variables on the Raman spectrum. This advancement is an informative step forward toward using SESORS for *in vivo* measurements and perhaps in clinically relevant environments.

EXPERIMENTAL SECTION

Instrumentation. Measurements were performed using an in-house built SORS system, based on the design by Shand and co-workers.[25] A 785 nm laser (Innovative Photonics Solutions) with attenuable output was coupled to one of two fiber-optic Raman probes (Wasatch Photonics) with built-in filtering optics. Raman probes were mounted on independent *xyz* translation stages with rotation mounts (ThorLabs) for precise and reproducible positioning and to provide a convenient means of directly measuring spatial offsets. A single probe was used in measurements with no spatial offset ($dx = 0$), whereas in SORS/SESORS measurements, both probes were utilized: probe 1 for excitation and probe 2 for collection. The two probes were angled at approximately 90° to each other. In each case, the collection probe is coupled to an f/1.3 Raman spectrometer (WP 785, Wasatch Photonics). In a typical experiment, spectra were collected for 100–1000 ms using a laser power of 400 mW. Raman spectra were processed using Igor Pro 6.3 (Wavemetrics) and Matlab 2014a (MathWorks). Spectral normalization and averaging were applied in specific instances.

Dark-field images were acquired using a 50×, 0.55 NA Nikon objective on an in-house microscope described elsewhere[26] and processed in ImageJ.[27] The images were processed by setting a threshold to distinguish particles from the background and using the "Analyze Particles" feature to calculate a percent area, which serves as a percent coverage of NP tags in the image.

Sample Preparation. A test sample for proof of concept and benchmarking experiments was made by curing vacuum-degassed polydimethylsiloxane (PDMS, Sylgard 184, Dow Corning) in a polystyrene (PS) cuvette at 60 °C for 3 h. This results in a sample with Raman spectra of the surface distinct from those of the subsurface.

Samples for SESORS experiments were prepared by spin-coating commercially available SERS NP solutions (originally supplied by Cabot Corp., Boston, MA, types S403, S421, and S440) on glass slides. Stock particles were centrifuged (500 μL, 6000 rpm, 20 min) and resuspended in 1000 μL of ethanol (Sigma-Aldrich), to a final dilution of 1:1. Glass slides (VWR) were rinsed in methanol (Sigma-Aldrich), dried under nitrogen, and treated in oxygen plasma for 1 min prior to being coated. Spin-coating was performed by dropping 20 drops of the NP solution onto the slide and spinning the slide at 2000 rpm for 60 s. The tissue analogues used in SESORS experiments were thinly sliced sections of pork belly, sliced to a thickness of 1.35 mm, purchased from a local market. Pork has been used in related work as a human tissue analogue.[18] Sections were cut into approximately 25 mm × 25 mm squares.

RESULTS AND DISCUSSION

Instrument Validation. The initial experiments performed with the SORS instrument, shown in Figure 1, were designed to confirm that the configuration did indeed result in SORS measurements. As described previously, a test sample of PDMS cured into a PS cuvette was prepared to provide a sample that is layered with spectrally distinct species, to obtain a "surface" spectrum at $dx = 0$, and a subsurface spectrum at an arbitrary $dx > 0$. As seen in Figure 2, the Raman spectrum of the cuvette alone with a single probe (a) matches the spectrum collected with both probes overlapped and no spatial offset (b; $dx = 0$ mm). There is clear spectral overlap between spectra a and b, evidenced by the presence of Raman peaks at 620, 1001, 1031, and 1602 cm^{-1}. When a spatial offset of 2 mm is applied to the collection probe, the spectrum obtained (c) compares favorably to the spectrum of pure PDMS collected with a single probe (d). Offset spectrum c shows stretches from the subsurface PDMS (487, 616, 709, and 1409 cm^{-1}), as well as a subtle trace of the surface (PS) layer, with a weak peak at 1001 cm^{-1}. This serves as confirmation that the system, as assembled, is allowing collection of SORS spectra and gathering of spectral information from a subsurface layer when an offset is applied in the *x*-direction.

DOI: 10.1021/acsami.7b09197
ACS Appl. Mater. Interfaces XXXX, XXX, XXX−XXX

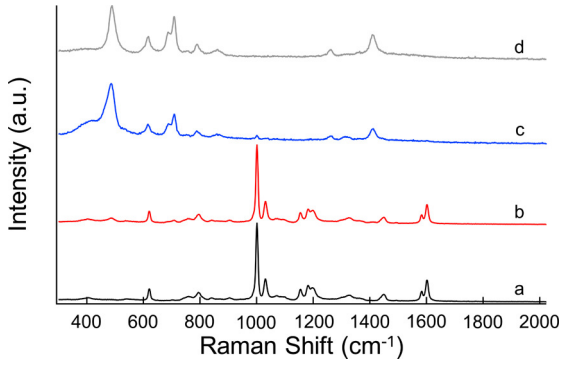

Figure 2. Comparison of the Raman spectra of (a) the polystyrene cuvette, (b) the test sample with no spatial offset ($dx = 0$), (c) the test sample with a spatial offset of 2.0 mm (i.e., $dx = 2.0$ mm), and (d) pure PDMS. Spectra are normalized and offset for the sake of clarity ($\lambda = 785$ nm; $t = 1000$ ms; one acquisition).

SESORS Sample Characterization. The spin-coated slides to be used in SESORS experiments were first characterized without tissue present to ensure a consistent NP distribution and a Raman signal across the surface of the slide. A representative summary of this characterization is shown in Figure 3. The samples were characterized in two, correlated ways; nine dark-field (DF) images and nine Raman spectra were collected on each slide at the positions shown in Figure 3a. Dark-field images were then processed in ImageJ by applying a threshold to the raw image and then using the "Analyze Particles" tool to measure the percentage area of NPs in the image, as shown in Figure 3b. Panel c shows the respective DF images collected at the positions indicated in panel a, while panel d shows the Raman spectra from these nine positions (in colored, dashed lines) and the averaged spectrum (solid black line). The images and spectra presented demonstrate that the distribution of particles and Raman intensity across the slide is relatively homogeneous when compared to results obtained by drop-casting particles, which can result in collections or voids of particles, as in the coffee ring-like distribution observed under common conditions.[28,29] This consistency will be of value when performing SESORS measurements, minimizing the potential for spectral variation that can be attributed to an inconsistent particle and Raman signal distribution. Also of note, the error (relative standard deviation) in the DF percentage area (16.6%) is greater than the error in the Raman intensity (13.4%); this result is consistent with what has been previously observed for two-dimensional, planar SERS substrates.[30]

SERS versus SESORS. After characterization of the spin-coated samples and validation of the SORS instrument, the initial experiments with coated slides and tissue analogues were performed. The first experiment was designed to show that for the detection of the NP signal from the substrate embedded in tissue, the use of two probes with a spatial offset (i.e., SESORS) provides an improvement over the use of a single probe with a change in axial focus through the tissue (SERS). In addition, this experiment is a means of demonstrating that the observed SESORS spectra are not merely a consequence of the change in axial focus (dz) as the angled probe is moved in the x-direction.

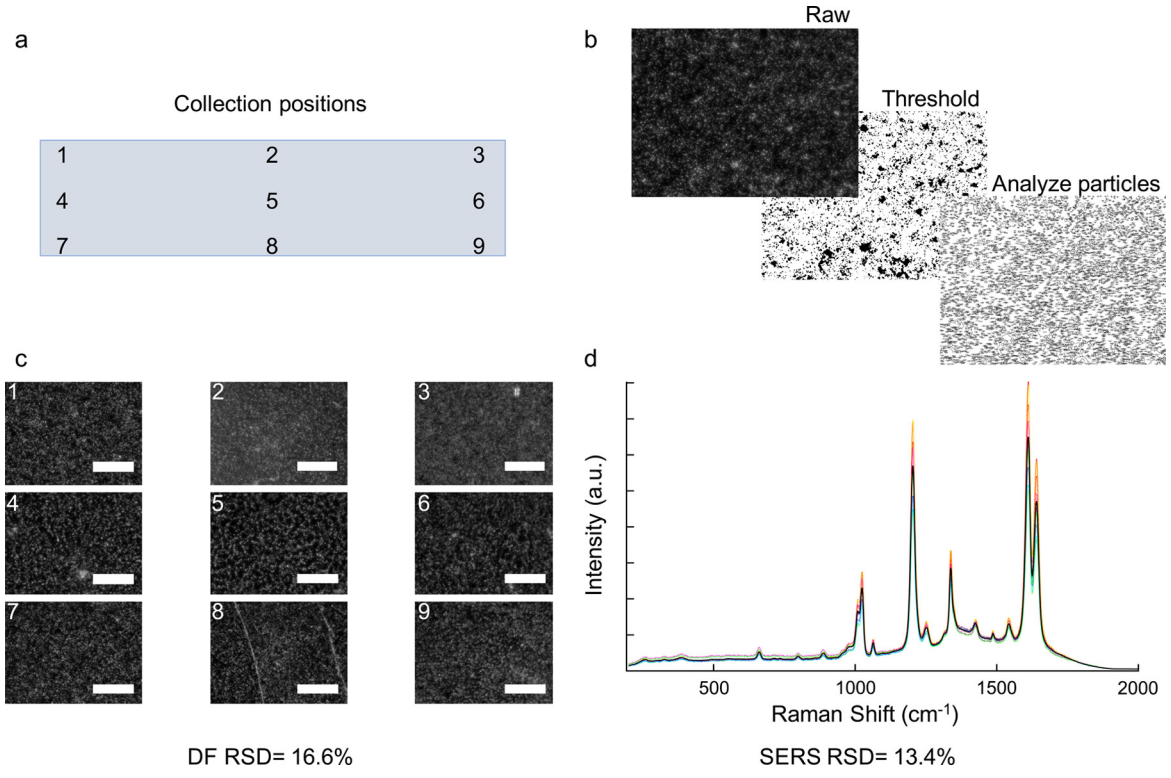

Figure 3. Characterization of type S440 SESORS samples via dark-field (DF) imaging and Raman spectroscopy. Measurements were taken at the indicated sample positions (a). Dark-field images were processed in ImageJ via thresholding and the "Analyze Particles" tool (b) to calculate the percent area of particle coverage. The DF images (c) show consistent particle coverage from the spin-coating process (16.6% RSD in the particle area). Raman spectra (d) at correlated positions (colored, dashed traces) show consistent Raman intensity (13.4% RSD) when compared to the average spectrum (solid black trace). DF: scale bar, 50 μm. Raman: $\lambda = 785$ nm; $t = 100$ ms; one acquisition.

DOI: 10.1021/acsami.7b09197
ACS Appl. Mater. Interfaces XXXX, XXX, XXX−XXX

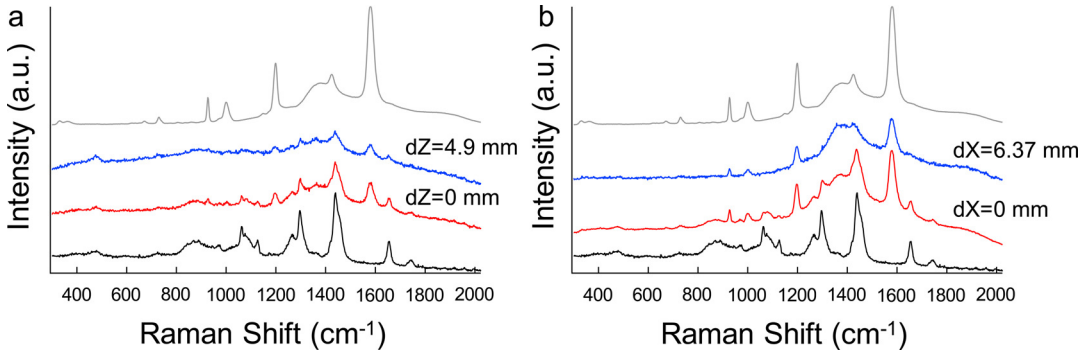

Figure 4. Comparison of (a) SERS (one probe) *z*-variation vs (b) SESORS (two probes) *x*-variation measurements with a constant thickness of tissue. The black and gray spectra are those of the pure tissue and nanoparticle (type S421), respectively, while the red spectra represent the zero-offset measurement (d*z* = 0; d*x* = 0). The blue spectrum in panel a represents a change (d*z* = 4.9 mm) in the *z*-direction for a single probe (change in only the focus), whereas the blue spectrum in panel b represents a change in the *x*-direction (d*x* = 6.37 mm) of the collection probe (SESORS). Spectra are normalized and offset for the sake of clarity (λ = 785 nm; *t* = 500 ms; one acquisition).

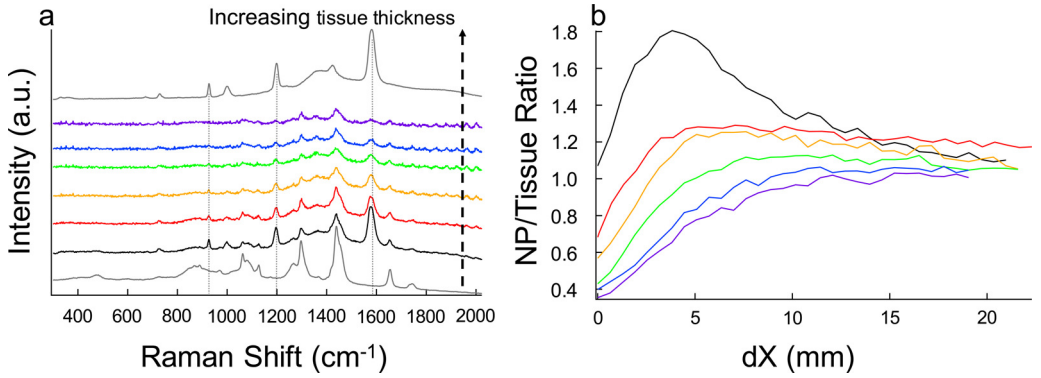

Figure 5. SESORS experiments with variable tissue thicknesses. Panel a shows reference spectra for the tissue (bottom, gray) and S421 NPs (top, gray) and spectra collected with increasing tissue thicknesses (black for 1.35 mm, red for 2.7 mm, orange for 4.05 mm, green for 5.40 mm, blue for 6.75 mm, and purple for 8.10 mm). Dotted sight lines are shown to indicate NP peak positions. Panel b shows the nanoparticle/tissue signal ratio (1580/1063 cm^{-1}) as a function of spatial offset (d*x*) in millimeters, with the colors corresponding to the same tissue thicknesses in panel a. The representative spectra in panel a are taken from the maximal point in the corresponding curve in panel b. All spectra are normalized and offset for the sake of clarity (λ = 785 nm; *t* = 500 ms; one acquisition).

To perform this comparison, a single layer of pork (1.35 mm thick) was placed on top of the NP-coated slide with a 1:1 dilution of S421 particles. For the single-probe experiment, the focus was adjusted via the micrometer in an attempt to focus through the surface layer (tissue) to obtain the signal from the subsurface (NPs on slide), whereas in the two-probe experiment, the probes were first overlapped by maximizing the surface signal and then the collection probe stepped off in the *x*-direction at regular intervals.

Representative spectra for both experiments are shown in Figure 4. In the single-probe experiment (a), an attempt to focus through the tissue onto the slide (d*z* = 4.9 mm) resulted in a relatively weak contribution from the NPs on the slide below (peaks at 1198 and 1581 cm^{-1}) and a spectrum that is more representative of the surface (i.e., tissue) spectrum (stretches at 1297, 1438, and 1656 cm^{-1}). However, in the two-probe experiment, the application of a spatial offset (d*x* = 6.37 mm) was shown to diminish the signal obtained from the surface layer (tissue), increasing the relative spectral contribution from the subsurface layer (NPs) as expected in a SORS or, in this instance, SESORS measurement. In addition to the NP signal, a spectral contribution is observed from the glass slide between 1300 and 1500 cm^{-1}, similar to what is observed in the reference spectrum from the SESORS sample. This confirms that for the measurement at hand, the two-probe SESORS collection configuration delivers drastically improved results compared to the measurements made with a single probe and variable axial focus.

Tissue Thickness in SESORS Experiments. With the SESORS measurement methodology established, the limits of tissue thickness were tested by adding multiple layers of tissue. In these experiments, layers of tissue were built upon the NP-coated slide (S421, 1:1 dilution) to obtain thicknesses ranging from 1.35 to 8.10 mm. As before, spectra were collected at regular intervals as the spatial offset ($n \geq 30$ steps; ~0.6 mm/step) was applied. The results of these experiments are shown in Figure 5.

Figure 5a shows reference spectra from the tissue (bottom) and NP S421 (top) in gray and representative spectra of tissue at varied thicknesses. The spectra correspond to increasing thicknesses of tissue: black for 1.35 mm, red for 2.7 mm, orange for 4.05 mm, green for 5.40 mm, blue for 6.75 mm, and purple for 8.10 mm. As shown in Figure 5a, all Raman signals become weaker as the tissue thickness is increased; the nanoparticle signal can be obtained to a thickness of 6.75 mm, with a diminished contribution from the surface layer. This is encouraging for *in vivo* work, as the average human skin thickness is on the order of 1−5 mm.

A peak ratio of NP to tissue (1580/1063 cm^{-1}) was used to measure the relative contribution of NPs to tissue in a given

DOI: 10.1021/acsami.7b09197
ACS Appl. Mater. Interfaces XXXX, XXX, XXX−XXX

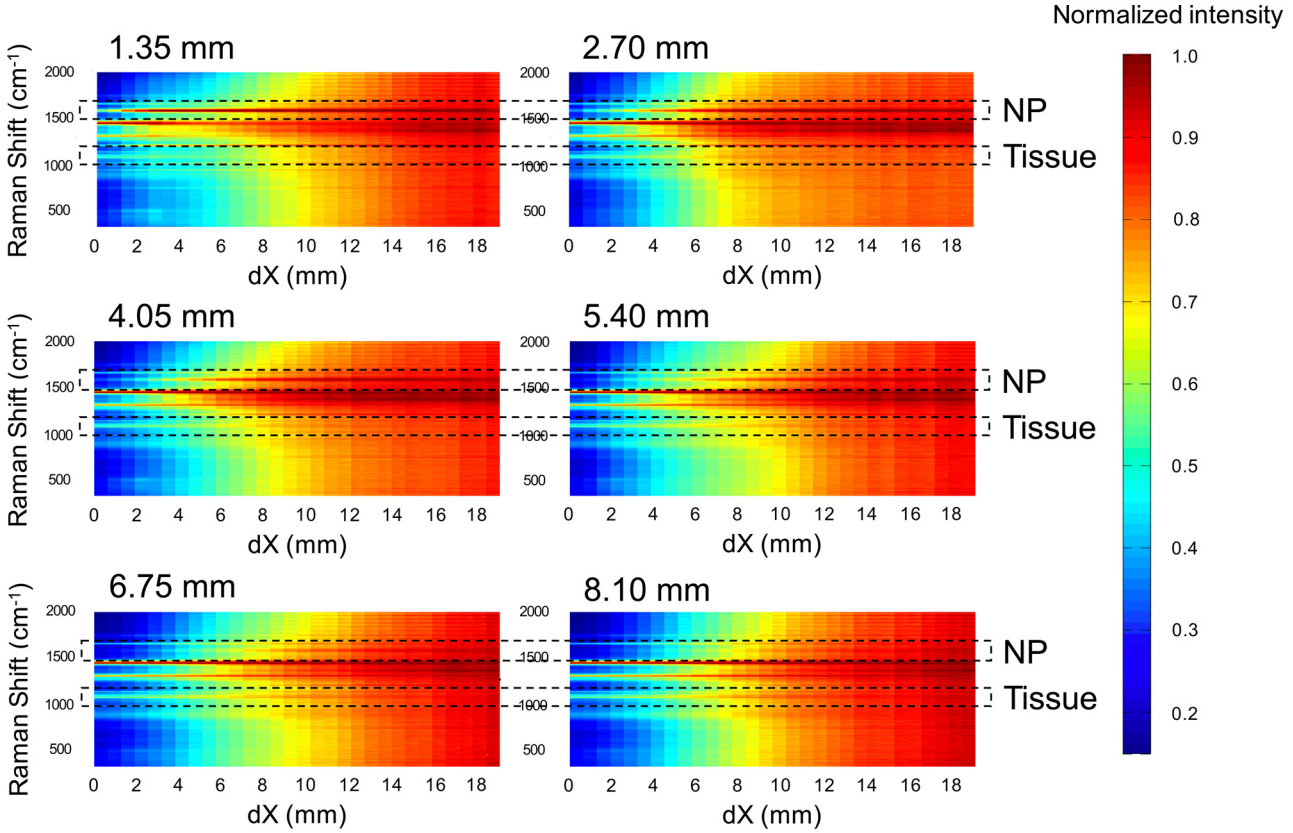

Figure 6. Series of heat maps showing the change in normalized spectral intensity (blue to red scale) as a function of Raman Shift (cm^{-1}, *y*-axis), spatial offset (d*x* in millimeters, *x*-axis), and tissue thickness (thickness in millimeters). Visual aids have been added to highlight Raman frequencies associated with both the tissue and subsurface S421 NPs. Notable features are the increase in d*x* required to obtain a NP-dominated spectrum as the tissue thickness increases and the incongruous trends in normalized intensity between the peak associated with the tissue section (1063 cm^{-1}), which is generally consistent, and the highly sensitive peak of the NPs (1580 cm^{-1}) (λ = 785 nm; t = 500 ms; one acquisition).

spectrum. The representative spectra shown in Figure 5a are taken from the maxima for the curves in Figure 5b. Figure 5b shows the NP/tissue ratio (peaks at 1580/1063 cm^{-1}, respectively) as a function of ≥30 spatial offsets (d*x*); 1063 cm^{-1} was selected as a tissue signal to avoid contributions from the aforementioned glass interference between 1300 and 1500 cm^{-1}. Generally, the ratio increases as a function of d*x* and then gradually falls off, approaching 1 at large offsets, where the spectra are dominated by noise. These curves show that as the tissue thickness increases, the spatial offset required to obtain the maximal NP/tissue signal ratio also increases. In other words, the greater the tissue thickness, the greater the spatial offset needed to obtain the signal from the subsurface nanotags. While perhaps intuitive, this conclusion can be credibly reached only by explicitly measuring the effects on the Raman spectrum of both the spatial offset and the tissue thickness.

The data in Figure 5 can also be represented as a series of three-dimensional heat maps, shown in Figure 6. The figure shows the normalized spectral intensity (blue to red color scale) as a function of Raman shift (cm^{-1}, *y*-axis), spatial offset (d*x* in millimeters, *x*-axis), and tissue thickness (total section thickness shown in millimeters). At the Raman frequencies of interest (1063 and 1580 cm^{-1} for the tissue and S421 NPs, respectively), the spectral intensity varies disparately as a function of both spatial offset and tissue thickness. The peak associated with the tissue is consistent across the measurements and largely insensitive to the increase in tissue thickness, showing only a slight increase in normalized intensity at greater tissue thicknesses and large d*x* values. On the other hand, the peak associated with the NPs is highly sensitive, showing drastic variance with respect to both of the aforementioned variables. At a small tissue thickness (1.35 mm), the peak dominates the normalized spectrum at all measured spatial offsets, at d*x* values from approximately 2 to 18 mm. As the tissue thickness increases through the frames, we see a marked increase in the onset of NP signal dominance of the spectrum when considering the spatial offset; that is, as the tissue thickness increases, a greater spatial offset is required to obtain spectra with a relatively large NP contribution. This is the same trend observed in Figure 5b. In addition, as the tissue thickness increases, the width (in d*x*) over which the NP spectrum dominates is narrowed. Finally, the last frame demonstrates limits of this methodology as described. For a sufficiently large tissue section (8.10 mm), very little Raman intensity associated with NPs is observed, and for all tissue thicknesses, at a sufficiently large d*x*, the spectrum becomes flattened and is dominated by noise.

CONCLUSION AND FUTURE DIRECTIONS

This work shows an unprecedented advancement forward for SESORS in that it demonstrates the use of the methodology in a backscattering geometry with spin-coated NP tags, a layer-by-layer analysis of tissue thickness to determine the system's limits, and the importance of modulating the spatial offset as a function of tissue thickness to maximize the NP tag signal. The configuration herein allows for the study of the interrelated

DOI: 10.1021/acsami.7b09197
ACS Appl. Mater. Interfaces XXXX, XXX, XXX−XXX

effects of the spatial offset and tissue thickness. It also makes SESORS more applicable when compared to previous work with tissue and NPs as an enhancing medium, which was performed with either a single or extreme (180°) spatial offset. With SERS tags uniformly coated on a glass slide as the subsurface material, the signal could be attained without undue data processing or treatment at a tissue thickness of 6.75 mm, helping to open the possibility of further SESORS measurements *in vivo*. To date, this work addresses only one of the practical limits of the technique, depth; this boundary can and will be pushed forward with more sensitive particles, elegant instrument design, and technological developments. Additionally, other frontiers for investigation in SESORS exist, such as establishing a minimal NP concentration for detection at a given tissue thickness and further optimization and demonstration of the technique for *in vivo* analysis.

AUTHOR INFORMATION

Corresponding Author

*E-mail: duncan.graham@strath.ac.uk.

ORCID

Steven M. Asiala: 0000-0002-3517-9915

Notes

The authors declare no competing financial interest.

Raw data associated with the results shown are accessible at http://dx.doi.org/10.15129/476eb716-6bd0-471b-8d28-045c42fb7aa2.

ACKNOWLEDGMENTS

The authors acknowledge the support of the EPSRC (EP/L014165/1). Additionally, S.M.A. acknowledges Dr. Christopher Steven, Dr. Samuel Mabbott, and Benjamin Breig for their respective contributions.

REFERENCES

(1) Stiles, P. L.; Dieringer, J. A.; Shah, N. C.; Van Duyne, R. R. Surface-Enhanced Raman Spectroscopy. *Annu. Rev. Anal. Chem.* **2008**, *1*, 601−626.

(2) Kneipp, K.; Kneipp, H.; Bohr, H. G. Single-molecule SERS Spectroscopy. *Top Appl. Phys.* **2006**, *103*, 261−277.

(3) Zrimsek, A. B.; Wong, N. L.; Van Duyne, R. P. Single Molecule Surface-Enhanced Raman Spectroscopy: A Critical Analysis of the Bianalyte versus Isotopologue Proof. *J. Phys. Chem. C* **2016**, *120* (9), 5133−5142.

(4) Hao, E.; Schatz, G. C. Electromagnetic Fields Around Silver Nanoparticles and Dimers. *J. Chem. Phys.* **2004**, *120* (1), 357−366.

(5) Qian, X.; Peng, X. H.; Ansari, D. O.; Yin-Goen, Q.; Chen, G. Z.; Shin, D. M.; Yang, L.; Young, A. N.; Wang, M. D.; Nie, S. In Vivo Tumor Targeting and Spectroscopic Detection with Surface-enhanced Raman Nanoparticle Tags. *Nat. Biotechnol.* **2008**, *26* (1), 83−90.

(6) McQueenie, R.; Stevenson, R.; Benson, R.; MacRitchie, N.; McInnes, I.; Maffia, P.; Faulds, K.; Graham, D.; Brewer, J.; Garside, P. Detection of Inflammation In Vivo by Surface-enhanced Raman Scattering Provides Higher Sensitivity Than Conventional Fluorescence Imaging. *Anal. Chem.* **2012**, *84* (14), 5968−75.

(7) Dinish, U. S.; Balasundaram, G.; Chang, Y. T.; Olivo, M. Actively Targeted In Vivo Multiplex Detection of Intrinsic Cancer Biomarkers Using Biocompatible SERS Nanotags. *Sci. Rep.* **2015**, *4*, 4075.

(8) Mohs, A. M.; Mancini, M. C.; Singhal, S.; Provenzale, J. M.; Leyland-Jones, B.; Wang, M. D.; Nie, S. M. Hand-held Spectroscopic Device for In Vivo and Intraoperative Tumor Detection: Contrast Enhancement, Detection Sensitivity, and Tissue Penetration. *Anal. Chem.* **2010**, *82* (21), 9058−9065.

(9) Bohndiek, S. E.; Wagadarikar, A.; Zavaleta, C. L.; Van de Sompel, D.; Garai, E.; Jokerst, J. V.; Yazdanfar, S.; Gambhir, S. S. A Small Animal Raman Instrument for Rapid, Wide-area, Spectroscopic Imaging. *Proc. Natl. Acad. Sci. U. S. A.* **2013**, *110* (30), 12408−12413.

(10) McVeigh, P. Z.; Mallia, R. J.; Veilleux, I.; Wilson, B. C. Widefield Quantitative Multiplex Surface Enhanced Raman Scattering iImaging In Vivo. *J. Biomed. Opt.* **2013**, *18* (4), 046011.

(11) Jeong, S.; Kim, Y. I.; Kang, H.; Kim, G.; Cha, M. G.; Chang, H.; Jung, K. O.; Kim, Y. H.; Jun, B. H.; Hwang, D. W.; Lee, Y. S.; Youn, H.; Lee, Y. S.; Kang, K. W.; Lee, D. S.; Jeong, D. H. Fluorescence-Raman Dual Modal Endoscopic System for Multiplexed Molecular Diagnostics. *Sci. Rep.* **2015**, *5*, 9455.

(12) Dong, J.; Chen, Q. F.; Rong, C. H.; Li, D. Y.; Rao, Y. Y. Minimally Invasive Surface-Enhanced Raman Scattering Detection with Depth Profiles Based on a Surface-Enhanced Raman Scattering-Active Acupuncture Needle. *Anal. Chem.* **2011**, *83* (16), 6191−6195.

(13) Matousek, P.; Morris, M. D.; Everall, N.; Clark, I. P.; Towrie, M.; Draper, E.; Goodship, A.; Parker, A. W. Numerical Simulations of Subsurface Probing in Diffusely Scattering Media Using Spatially Offset Raman Spectroscopy. *Appl. Spectrosc.* **2005**, *59* (12), 1485−1492.

(14) Matousek, P.; Clark, I. P.; Draper, E. R. C.; Morris, M. D.; Goodship, A. E.; Everall, N.; Towrie, M.; Finney, W. F.; Parker, A. W. Subsurface Probing in Diffusely Scattering Media Using Spatially Offset Raman Spectroscopy. *Appl. Spectrosc.* **2005**, *59* (4), 393−400.

(15) Schulmerich, M. V.; Cole, J. H.; Kreider, J. M.; Esmonde-White, F.; Dooley, K. A.; Goldstein, S. A.; Morris, M. D. Transcutaneous Raman Spectroscopy of Murine Bone In Vivo. *Appl. Spectrosc.* **2009**, *63* (3), 286−295.

(16) Matousek, P.; Draper, E. R. C.; Goodship, A. E.; Clark, I. P.; Ronayne, K. L.; Parker, A. W. Noninvasive Raman Spectroscopy of Human Tissue In Vivo. *Appl. Spectrosc.* **2006**, *60* (7), 758−763.

(17) Stone, N.; Faulds, K.; Graham, D.; Matousek, P. Prospects of Deep Raman Spectroscopy for Noninvasive Detection of Conjugated Surface Enhanced Resonance Raman Scattering Nanoparticles Buried within 25 mm of Mammalian Tissue. *Anal. Chem.* **2010**, *82* (10), 3969−3973.

(18) Stone, N.; Kerssens, M.; Lloyd, G. R.; Faulds, K.; Graham, D.; Matousek, P. Surface Enhanced Spatially Offset Raman Spectroscopic (SESORS) Imaging - The Next Dimension. *Chem. Sci.* **2011**, *2* (4), 776−780.

(19) Xie, H. N.; Stevenson, R.; Stone, N.; Hernandez-Santana, A.; Faulds, K.; Graham, D. Tracking Bisphosphonates through a 20 mm Thick Porcine Tissue by Using Surface-Enhanced Spatially Offset Raman Spectroscopy. *Angew. Chem., Int. Ed.* **2012**, *51* (34), 8509−8511.

(20) Dey, P.; Olds, W.; Blakey, I.; Thurecht, K. J.; Izake, E. L.; Fredericks, P. M. SERS-based Detection of Barcoded Gold Nanoparticle Assemblies from Within Animal Tissue. *J. Raman Spectrosc.* **2013**, *44* (12), 1659−1665.

(21) Dey, P.; Olds, W.; Blakey, I.; Thurecht, K. J.; Izake, E. L.; Fredericks, P. M. SERS-barcoded Colloidal Gold NP Assemblies as Imaging Agents for use in Biodiagnostics. *Proc. SPIE* **2014**, 89390A.

(22) Yuen, J. M.; Shah, N. C.; Walsh, J. T., Jr.; Glucksberg, M. R.; Van Duyne, R. P. Transcutaneous Glucose Sensing by Surface-enhanced Spatially Offset Raman Spectroscopy in a rat model. *Anal. Chem.* **2010**, *82* (20), 8382−5.

(23) Ma, K.; Yuen, J. M.; Shah, N. C.; Walsh, J. T.; Glucksberg, M. R.; Van Duyne, R. P. In Vivo, Transcutaneous Glucose Sensing Using Surface-Enhanced Spatially Offset Raman Spectroscopy: Multiple Rats, Improved Hypoglycemic Accuracy, Low Incident Power, and Continuous Monitoring for Greater than 17 Days. *Anal. Chem.* **2011**, *83* (23), 9146−9152.

(24) Sharma, B.; Ma, K.; Glucksberg, M. R.; Van Duyne, R. P. Seeing Through Bone with Surface-Enhanced Spatially Offset Raman Spectroscopy. *J. Am. Chem. Soc.* **2013**, *135* (46), 17290−17293.

(25) Hopkins, R. J.; Pelfrey, S. H.; Shand, N. C. Short-wave Infrared Excited Spatially Offset Raman Spectroscopy (SORS) for Through-barrier Detection. *Analyst* **2012**, *137* (19), 4408−4410.

(26) McLintock, A.; Cunha-Matos, C. A.; Zagnoni, M.; Millington, O. R.; Wark, A. W. Universal Surface-Enhanced Raman Tags:

DOI: 10.1021/acsami.7b09197
ACS Appl. Mater. Interfaces XXXX, XXX, XXX−XXX

Individual Nanorods for Measurements from the Visible to the Infrared (514−1064 nm). *ACS Nano* **2014**, *8* (8), 8600−8609.
(27) Schneider, C. A.; Rasband, W. S.; Eliceiri, K. W. NIH Image to ImageJ: 25 Years of Image Analysis. *Nat. Methods* **2012**, *9* (7), 671−675.
(28) Deegan, R. D.; Bakajin, O.; Dupont, T. F.; Huber, G.; Nagel, S. R.; Witten, T. A. Capillary Flow as the Cause of Ring Stains from Dried Liquid Drops. *Nature* **1997**, *389* (6653), 827−829.
(29) Li, Y. N.; Yang, Q.; Li, M. Z.; Song, Y. L. Rate-dependent Interface Capture Beyond the Coffee-ring Effect. *Sci. Rep.* **2016**, *6*, 24628.
(30) Asiala, S. M.; Schultz, Z. D. Characterization of Hotspots in a Highly Enhancing SERS Substrate. *Analyst* **2011**, *136* (21), 4472−4479.

DOI: 10.1021/acsami.7b09197
ACS Appl. Mater. Interfaces XXXX, XXX, XXX−XXX